THE JOURNAL OF PHYSICAL CHEMISTRY B
A JOURNAL OF THE AMERICAN CHEMICAL SOCIETY

pubs.acs.org/JPCB

Article

Free-Energy Landscape of the S_N2 Reaction $CH_3Br + Cl^- \rightarrow CH_3Cl + Br^-$ in Different Liquid Environments

Danillo Valverde,* Herbert C. Georg, and Sylvio Canuto

Cite This: *J. Phys. Chem. B* 2022, 126, 3685−3692

Read Online

ACCESS | Metrics & More | Article Recommendations | Supporting Information

ABSTRACT: This work describes in detail the reaction path of the well-known S_N2 reaction $CH_3Br + Cl^- \rightarrow CH_3Cl + Br^-$, whose reaction rate has a huge variation with the solvent in the gas phase and in protic and aprotic liquid environments. We employed the ASEC-FEG method to optimize for minima (reactants and products) and saddle points (transition states) in the in-solution free-energy hypersurface. The method takes atomistic details of the solvent into account. A polarizable continuum model (PCM) has also been employed for comparison. The most perceptive structural changes are noted in aqueous solution by using the ASEC-FEG approach. The activation energies in all solvents, estimated by means of free-energy perturbation calculations, are in good agreement with the experimental data. The total solute−solvent hydrogen bonds play an important role in the increased barrier height observed in water and are therefore crucial to explain the huge decrease in the kinetic constant. It is also found that the hydration shell around the ions breaks itself spontaneously to accommodate the molecule, thus forming minimum energy complexes.

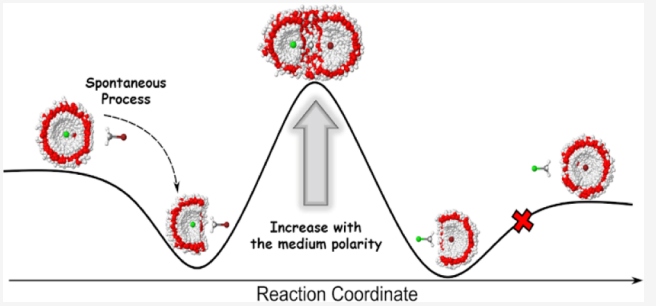

1. INTRODUCTION

Bimolecular nucleophilic substitution (S_N2) reactions play a fundamental role in the building of functional groups in organic chemistry and are prototypes of more complex bimolecular systems.[1−3] In view of these applications over the last decades, an enormous amount of experimental and/or theoretical works has been devoted to understanding the mechanisms behind these chemical reactions in the gas phase.[4−13] This type of reaction consists of a concerted process governed by the making and breaking of two single bonds on the α-carbon. In general, there is a consensus that the ground-state potential energy surface exhibits two deep minima, originated by the strong dipole-charge interaction, with a transition state barrier height separating them.[14−16] Another interesting feature is that their reaction rates are very affected by the surrounding environment and can drastically change in comparison with the gas phase. In particular, some reactions show rates that are 10 or more orders of magnitude smaller when taking place in water than in the gas phase.[17−19] This means that the activation barrier increases and, as a consequence, the reaction velocity is slower in solution. The solute−solvent hydrogen bonds formed in aqueous solution are important for understanding the increase in the barrier height as well as a better energetic stabilization of the minima.[20] In terms of theoretical predictions for the case in solution, most of the studies focus on describing the mechanism in water using microsolvation models.[13,21−25] Although some partial success might be obtained with microsolvation, it is well-timed to recognize that this approach ignores the characteristics of the liquid nature and the related thermodynamic condition. Noting this dearth of theoretical studies, we address here the explicit inclusion of the liquid solvent interaction and extend the study to include other solvents and solvent effects, both protic and aprotic.

Today, there are two well-consolidated manners to incorporate solvent effects. The first one is based on implicit solvation by treating the solvent as a dielectric or a conductor continuum,[26,27] which implies that the degrees of freedom (DOFs) of the solvent are neglected, and thus specific interactions cannot be taken into account. This approach has the great advantage of having a low computational cost, demanding almost the same computational time as considering only the isolated molecule. We aim at a procedure to remove some of the limitations of implicit solvation and to explicitly consider in the quantum mechanical calculation the nearest solvent molecules around the solute. The issue now is the number and position of the solvent molecules to be included. Those ones can be obtained with molecular simulation techniques with a specified thermodynamic condition. Among these approaches, we here highlight those that combine quantum mechanics (QM) methods and molecular mechanics

Received: December 3, 2021
Revised: April 27, 2022
Published: May 11, 2022

https://doi.org/10.1021/acs.jpcb.1c10282
J. Phys. Chem. B 2022, 126, 3685−3692

(MM) simulations, namely QM/MM methods.[28] In this context, some of us have previously developed a methodology that allows optimizing the free energy of molecules in solution by using a sequential QM/MM methodology[29] (S-QM/MM) and the free-energy gradient[30,31] (FEG). An important point in this is the selection of the interacting potential, and we have used an average solvent electrostatic configuration (ASEC).[32] This has been coined as the ASEC-FEG method.[33,34] This approach has been shown to be relatively accurate to characterize free-energy minima as well as electronic properties of several molecules in solution for different electronic states.[35−38] The understanding of chemical reactions and the calculation of reaction rates require obtaining good potential energy surfaces and, in particular, some stationary points along the reaction paths. In a liquid situation, the thermodynamic condition plays a pivotal role, and it is thus of essential importance to consider the free energy and the solute−solvent interactions. Note that in the MM part, either molecular dynamics (DM) or Monte Carlo simulation techniques can be, in principle, applied since both are able to generate a representative sample of the configuration space. We have chosen MC because our focus of study does not include the evaluation of temporal properties and a smaller number of steps to achieve the equilibrium regime is required in MC.[39]

In this work, we thus apply the promising ASEC-FEG approach to investigate an important and, in most cases, an essential point in the study of chemical reaction in solution, the transition states (TS). Inspired by this motivation, we have selected the well-known S_N2 $CH_3Br + Cl^- \rightarrow CH_3Cl + Br^-$ reaction, whose solvent effects are enormously pronounced and therefore are a good challenge to any theoretical method. This specific reaction is very sensitive to the environment and its kinetic constant varies from vacuum to water by more than 10 orders of magnitude, which in terms of the free-energy difference represents a barrier increase of around 15 kcal/mol.[40−42] Up until now, this reaction has been extensively studied theoretically in the gas phase[4,5,43,44] and only a few theoretical studies have addressed it in aqueous solution.[45,46] Nonetheless, the reaction rate drops sharply in aprotic solvents,[47−49] and up to date, we have found no theoretical studies dedicated to the subject and hence no theoretical analysis of this reaction rate. Therefore, we propose to systematically investigate this S_N2 reaction in aqueous solution as well as in two other solvents (acetone and dimethylformamide). Accordingly, several ground-state critical points are optimized in the gas phase and in solution, and their free energy is estimated. Finally, the energetic and entropic contributions along the reaction path are obtained and discussed in some detail.

2. COMPUTATIONAL DETAILS

Ground-state critical points of $CH_3Br + Cl^- \rightarrow CH_3Cl + Br^-$ reaction were optimized, both in the gas phase and in solution, by using the second-order Møller−Plesset perturbation theory (MP2)[50] with the augmented triple-ζ atomic basis set (aug-cc-pVTZ).[51] This level of theory was chosen because it provides a good compromise between the agreement with the experimental activation energy value in the gas phase and computing time, besides being consistent with other highly correlated wave-function methods and larger atomic basis sets (see Tables S1 and S2 in Supporting Information). The increase in the basis sets from aug-cc-pVTZ to aug-cc-pQTZ or aug-cc-5TZ makes only a slight change in the relative energies of the critical points, differing by less than 1 kcal/mol. On comparing MP2 with MP4 and CCSD(T), the same trend is observed. Thus, we decided on a more economical MP2/aug-cc-pVTZ level. Harmonic vibrational frequency calculations indicated that the TS is correctly characterized as containing a single imaginary frequency which encompasses the motion of both ions in relation to the methyl group. Additionally, no imaginary frequencies were observed in the reactant and product structures, confirming that these geometries correspond to energetic minima in the ground-state surface.

Solvent effects were introduced with two schemes: (i) a simple implicit solvation with the self-consistent reaction field (SCRF) approach and the polarizable continuum model within the integral equation formalism (IEFPCM)[26] model and (ii) the more involved and accurate ASEC-FEG[33,34] approach. The latter one requires an iterative process where each optimization step consists of a classical simulation followed by QM calculations of the atomic forces and an adjustment of the charges on the atomic sites to update the solute electronic polarization by the solvent. The solute−solvent interaction in the QM part is inserted as a one-electron term in the solute's Hamiltonian by using an average solvent electrostatic embedding (ASEC)[32] for the solvent. In a similar fashion, Aguilar and co-workers proposed a scheme based on the average electrostatic potential instead of the average electrostatic configuration.[52] We refer interested readers to refs 32, 33, and 53 for more detailed information about the theory.

Classical simulations were performed using the MC method with Metropolis sampling.[54] Periodic boundary conditions, minimum-image convention, and long-range correction were applied in a cubic simulation box with a minimum solvation shell thickness of at least 12 Å, leading to 250 acetone (ACE) and dimethylformamide (DMF) molecules and 1000 water (WAT) molecules. Solvent and solute structures were treated as rigid along with the classical simulations. At each MC step, the molecular interaction is expressed as a sum of the Lennard-Jones (LJ) plus Coulomb potential over all atomic sites. For the solute, the LJ parameters were taken from the optimized potentials for liquid simulation (OPLS-AA),[55] while the set of initial atomic charges was calculated from a Merz−Singh−Kollman[56] (MK) fit using the same level of theory employed in the geometry optimization procedure. No van der Waals radius was requested to compute the partial charges on the chlorine and bromine ions. Specific force fields were adopted for ACE,[57] DMF,[58] and WAT.[59] The thermalization procedure is divided into two stages, which start with an *NVT* simulation of 8×10^4 MC steps per molecule and then an *NPT* simulation of 12×10^4 MC steps per molecule. Next, a production of 4×10^5 MC steps per molecule is carried out in the equilibrium regime. A total of 200 statistically uncorrelated configurations are stored to generate the ASEC electrostatic embedding, meaning that in each interval of 2×10^3 MC cycles, a configuration is saved. This interval was estimated by the biexponential fit of the energy autocorrelation function.[60] Normal conditions (T = 298 K and P = 1 atm) were adopted in the classical simulations. In the IEFPCM model, the adopted dielectric constants were 20.493, 37.781, and 78.355 for ACE, DMF, and WAT, respectively.

In order to obtain the Gibbs free-energy difference (ΔG), other MC simulations were performed employing the free-energy perturbation (FEP)[61] technique, connecting some points on the ground-state free-energy surface by interpolating geometry and atomic charges of the solute. Double-wide sampling[57] is employed in an effort to reduce the simulation time, implying that one simulation yields two increments in the

https://doi.org/10.1021/acs.jpcb.1c10282
J. Phys. Chem. B 2022, 126, 3685−3692

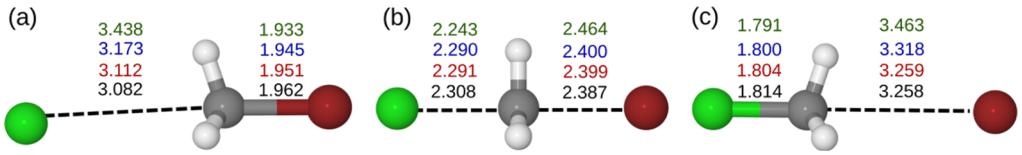

Figure 1. Optimized structure of the reaction complex in its (a) reactant, (b) TS, and (c) product species in the gas phase. The Cl−C and Br−C bond distances in the gas phase (black), acetone (red), dimethylformamide (blue), and water (green) are reported. Atomic representation: Cl = green, Br = dark red, C = gray, and H = white.

Gibbs free-energy change. The total ΔG is given by summing, in addition to the contribution estimated from FEP, the energetic difference due to the structural changes. For each one of these simulations, a total of 8×10^5 MC steps were run to reach a sufficiently small fluctuation of the ΔG value. Three independent simulations were carried out to get the standard deviation. This quantity was also predicted with the IEFPCM model, including the thermodynamic effects *via* vibrational frequency calculations. The MC classical simulations and the FEP calculations in the solvated environments were computed by using the DICE[62] code. All electronic structure calculations were carried out in the Gaussian 09[63] suite.

3. RESULTS AND DISCUSSION

3.1. Critical Points and Charge Distributions. In the gas phase, the Cl···C optimized length is 3.082 and 1.814 Å for reactant and product minima, respectively. On the other hand, the Br···C distance is calculated to be 1.962 and 3.258 Å, respectively. Both ions are nearly equidistant from the methyl group in the TS structure. Furthermore, in all stages of the reaction mechanism, the pair of ions remains colinear, with the angle formed by the Cl, C, and Br atoms close to 180°. These findings are consistent with previous theoretically coupled cluster calculations including perturbative triple excitations (CCSD(T))[4,5] and ab initio molecular dynamics using the density functional theory (DFT) and BLYP as functional.[6]

We have sought equivalent critical points in the ground-state free-energy surface in solution. Figure 1 shows the converged values of the Cl−C and Br−C bond distances in gas and solvent phases using the ASEC-FEG approach for the $CH_3Br + Cl^- \rightarrow CH_3Cl + Br^-$ reaction in its reactant, TS, and product structures. Solvent effects on the other coordinates are less pronounced.

In the reactant and product cases, the bond between the methyl group and the ion bonded to it, coined here as CH_3X (X = Br for reactant, and X = Br for product), decreases as the polarity of the medium increases. In relation to the gas phase, the largest change in this coordinate is observed for the reactant in water, reducing to about 0.030 Å its length. Conversely, the other ion moves away from the CH_3X group, mainly in aqueous solution. Even though the ion is far enough away from the CH_3X group, a full solvation shell around the ion is not verified.

Considering the transition state, the effects on the molecular structure are mild when the system is embedded in solutions of ACE or DMF. Again, the most perceptible changes occur in WAT, with the Cl···C bond shortening by 0.066 Å and the Br···C bond lengthening by 0.077 Å in relation to the gas phase. The values reported in water agree with those earlier obtained by Raugei *et al.* using Car−Parrinello molecular dynamics (CPMD) simulations[45] and other theoretical work of similar reactions.[20,64,65]

For comparison, we have also optimized all structures with the IEFPCM model. These results are shown in Table S3 in the Supporting Information. Overall, it predicts essentially the same structure in all solvents, which entails that the implicit solvation method cannot distinguish a solvent from another. This could be expected since no significant variation in the structure is noted from a certain value of the dielectric constant value. Besides, the Cl−C and Br−C bond distances are quite distinct from those optimized with the ASEC-FEG approach, predominantly in the aprotic solvent (ACE and DMF).

We have also analyzed the solvent effects on the atomic charge distribution (see Table 1). Here, we have only reported the values obtained from the ASEC-FEG approach. In both reactant and product, the inclusion of the solvent provokes a charge migration from the X halogen atom to the methyl group. In the TS structure, the atomic charge on the halogen atoms and the methyl group is significantly affected only in water, becoming more negative and positive, respectively. Recently, a theoretical study of the $FCH_3 + CN^- \rightarrow CH_3CN + F^-$ reaction in water[65] using an electrostatic DFT/MM embedding approach reported that along with the reaction, the halogen atom always has a negative charge (−0.36*e* for the reactant, −0.52*e* for TS, and −0.20*e* for the product), and the methyl group always has a positive charge (0.33*e* for the reactant, 0.34*e* for TS, and 0.20*e* for the product), which is well consistent with our theoretical predictions, even though the reaction is not the same.

Table 1. Charge Distribution (e) Over the Sites of the Reaction Complex in the Gas Phase, Acetone, Dimethylformamide, and Water

	site	GAS	ACE	DMF	WAT
reactant	C	−0.55	−0.67	−0.70	−0.78
	H	0.26	0.29	0.29	0.31
	Cl	−0.95	−0.97	−0.98	−1.02
	Br	−0.28	−0.23	−0.19	−0.13
TS	C	−0.49	−0.48	−0.49	−0.32
	H	0.29	0.28	0.29	0.29
	Cl	−0.70	−0.68	−0.69	−0.75
	Br	−0.68	−0.68	−0.69	−0.80
product	C	−0.33	−0.40	−0.43	−0.48
	H	0.20	0.21	0.22	0.24
	Cl	−0.29	−0.24	−0.23	−0.20
	Br	−0.98	−0.99	−1.00	−1.04

3.2. Solute−Solvent Hydrogen Bonds. The reaction complex only has acceptor sites, implying that solvent−solute hydrogen bonds (HB) can occur only in the case of water solution. Figure 2 shows the radial distribution function $g(r)$ between the halogen atoms of the complex and the oxygen atoms of water. As it can be noticed, the first peak and minimum positions of the $g(r)$ involving the Br and oxygen atoms are similar in the TS and the product, but this first peak is more intense in the product. The location of this sharp peak is a typical signature of HB, but additional criteria should be incorporated in order to better quantify the number of HBs (see below for

https://doi.org/10.1021/acs.jpcb.1c10282
J. Phys. Chem. B 2022, 126, 3685−3692

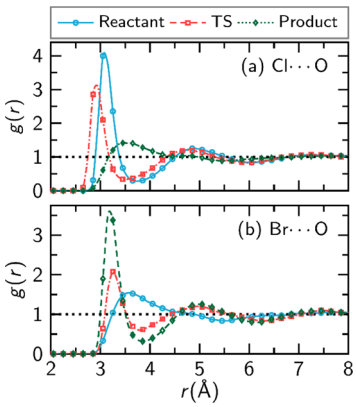

Figure 2. Radial distribution function between (a) chlorine in the solute and oxygen in water and (b) bromine in the solute and oxygen in water.

more details). The spherical integration over this first peak results in around seven and five water molecules surrounding the halogen atom in the product and TS structures, respectively. For the $g_{Cl-O}(r)$, the peaks and minima in the reactant are a little displaced with respect to the TS. However again, seven and four water molecules are found in the first shell around the chlorine atom for the reactant and TS structures, respectively. A previous CPMD study in water estimated a first solvation shell comprising, on an average, 3−4 water molecules around bromine in the TS structure,[46] which well fits with our results.

It cannot be assured that all water molecules located in this first peak are indeed associated with hydrogen bonds. Then, in this work, the number of HBs is obtained by using three complementary criteria:[66−68] (i) R_{XY}, which is defined by the first minimum of the $g(r)$ between the electronegative X and Y atoms; (ii) the θ_{XY} angle formed by the X, H, and Y atoms; and (iii) the binding energy (E_{HB}), which is determined from the histogram of the solute−solvent pairwise energy distribution. In this work, the selected parameters are $R_{Br-O} \leq 3.85$ Å, $R_{Cl-O} \leq 3.65$ Å, $\theta \leq 40°$, and $E_{HB} \leq -0.1$ kcal/mol. Table 2 exhibits the average number of hydrogen bonds (HB) that each halogen atom makes with the water and their respective classical interaction energy (ΔE).

Table 2. Average Number (HB) and Classical Average Interaction Energy (ΔE; kcal/mol) of Hydrogen Bonds Formed by $CH_3Br + Cl^-$ Reaction with the Water Molecules[a]

	reactant		TS		product	
	HB	ΔE	HB	ΔE	HB	ΔE
Cl···H−O	6.4	−12.0	4.4	−9.5	0.9	−2.8
Br···H−O	0.9	−2.3	4.3	−7.2	6.5	−10.9
C−H···O	0.2	−9.5	0.2	−5.8	0.3	−8.0
total	7.9	−85.0	9.3	−76.3	8.1	−79.3

[a]The total ΔE is computed as the sum of the interaction energy obtained at each electronegative site multiplied by its respective average number of HB.

The highest number of HBs is obtained in the TS stage, with an amount of 9.3 on average. However, the interaction energy due to them is the smallest. The reactant and product nearly make the same number of HBs (∼8), although the interaction energy coming from the HB is stronger in the reactant. In both minima, the halogen atom bound to the CH_3 group makes an equal number of HBs, which is less than 1. In turn, a similar number of HBs is observed for both halogen atoms in the TS structure. This result suggests that the increased barrier height in water, as compared to the gas phase or ACE or DMF solutions, is a consequence of weaker hydrogen bonding interactions in the TS structure than in either the reactant or product. This finding has been already observed previously in another S_N2 reaction.[69]

3.3. Energy Profile. The magnitude of the activation energy defines the speed at which the reaction occurs and can be quantified by the free-energy difference between the reactant and transition states. We have determined this property in vacuum by the inclusion of the vibrational effects and zero-energy contributions to the molecular Hamiltonian, whereas in a solvated environment, it has been evaluated by combining MC simulations and FEP technique (see section Computational Details). These results in all environments are shown in Table 3.

Table 3. Theoretical Activation Energy (kcal/mol) for the $CH_3Br + Cl^- \rightarrow CH_3Cl + Br^-$ Reaction in the Gas Phase and Three Solvents[a]

	GAS		
this work	10.5		
Exp.	8.6−10.7[40,41]		
	ACE	DMF	WAT
IEFPCM	21.1	21.8	22.7
FEP	13.9 ± 0.6	16.6 ± 0.2	24.2 ± 1.9
exp.	15.8[47]	17.9[48]	23.7[42]

[a]IEFPCM and FEP approaches were adopted to estimate the Gibbs free-energy difference between the reactant and TS structures in the solvent. Experimental data are also reported for comparison.

Our theoretical prediction for the reaction in vacuum is in good agreement with the available experimental measurements at T = 298 K.[40,41] Previous theoretical calculations at the CCSD(T)/cc-pVDZ level pointed to an activation energy value of 8.53 kcal/mol,[5] which is smaller than our results but could still be considered in good agreement with the experiment.

Experimental results show that the activation barrier from GAS to ACE is increased by around 5 kcal/mol. The results obtained using the FEP technique predict an increase of 3.4 kcal/mol, which differs from the experimental value by less than 2 kcal/mol. The experimental solvatochromic shift from ACE to DMF[47,48] indicates a moderate increase of 2.1 kcal/mol in the activation energy. Our theoretical result also reveals an increase that is computed to be 2.7 kcal/mol.

The largest experimental value for the activation energy is for the case of water, where its value is obtained as 23.7 kcal/mol.[42] We have found an activation barrier of 24.2 ± 1.9 kcal/mol using the FEP technique, which is in very good agreement with the experiment, with an essentially negligible difference of only 0.5 kcal/mol. From DMF to WAT, the experimental activation barrier increases by 5.8 kcal/mol, while the theoretical estimation is of 7.6 kcal/mol. In view of these results, we can conclude that the combination of the ASEC-FEG approach with the FEP technique is a good choice to obtain the activation barrier in solution and is able to well describe the energies involved in this nucleophilic reaction.

To our knowledge, unfortunately, theoretical studies of this nucleophilic reaction are limited to the water environment. However, in the case of the $CH_3Cl + CN^- \rightarrow CH_3CN + Cl^-$ reaction, Xu and co-workers[20] reported that the effects of water

https://doi.org/10.1021/acs.jpcb.1c10282
J. Phys. Chem. B 2022, 126, 3685−3692

and the polarization effect together increase the activation barrier height by around 11.4 kcal/mol based on multiscale QM/MM calculations, which is in accordance with our result (13.6 kcal/mol). Higashi and Truhlar[70] have also obtained a similar shift from gas to the aqueous solution for the $CH_3Cl + Cl^-$ reaction (~14 kcal/mol), employing a combination of DFT calculations and MD simulations.

It is worth mentioning that the IEFPCM approach describes well the activation energy in water (see Table 3). However, it fails in obtaining the distinction between different solvents, providing a similar activation energy value in the other solvents, leading to discrepancies compared to experiments of 5.3 and 3.9 kcal/mol for ACE and DMF, respectively.

The Gibbs free-energy difference between the reactant and product is also evaluated. Table 4 exhibits these calculated values using the same strategies as above. According to our results, the reaction is exothermic in the gas phase with the product being placed 4.6 kcal/mol below the reactant, which agrees with CCSD(T) calculations reported previously that obtained a value of −6.5 kcal/mol.[4]

Table 4. Difference in the Gibbs Free Energy between the Reactant and Product (kcal/mol) in Acetone, Dimethylformamide, and Water for the $CH_3Br + Cl^- \rightarrow CH_3Cl + Br^-$ Reaction

	ACE	DMF	WAT
IEFPCM	−1.5	−1.2	−1.2
FEP	−1.3 ± 0.9	−1.0 ± 0.3	−1.8 ± 2.2

The reaction remains exothermic in solution despite having less stability favoring the product, lowering by about 3 kcal/mol (see Table 4). In the case of water, for instance, the reaction is exothermic by about 2 kcal/mol. This behavior could be expected since the total solute−solvent hydrogen bonding interaction is stronger in the reactant. The IEFPCM model gives similar differences, as can also be seen in Table 4. These findings differ from those obtained previously[6] using the microsolvation technique with only one or two water molecules, where a greater stabilization in water (~7 kcal/mol) is suggested. Unfortunately, no experimental data have been found to make a comparison, but the limitations of the microsolvation model are clearly seen.

Finally, in Figure 3 are illustrated all the reaction processes for the $CH_3Br + Cl^- \rightarrow CH_3Cl + Br^-$ reaction in water. The energetic profile for the other solvents is also depicted. All these Gibbs free-energy differences are estimated using the FEP technique.

In all the solvents studied, the ion is not totally involved by a full solvation shell in the minima structure points (reactant and product), as stated before. A complete solvation shell is achieved by stretching the $CH_3\cdots Y$ distance around 6 Å in WAT and 10 Å for ACE and DMF. FEP calculations predict that these two structures are energetically located more than 10 kcal/mol above the nearest minimum. This difference is larger in acetone and

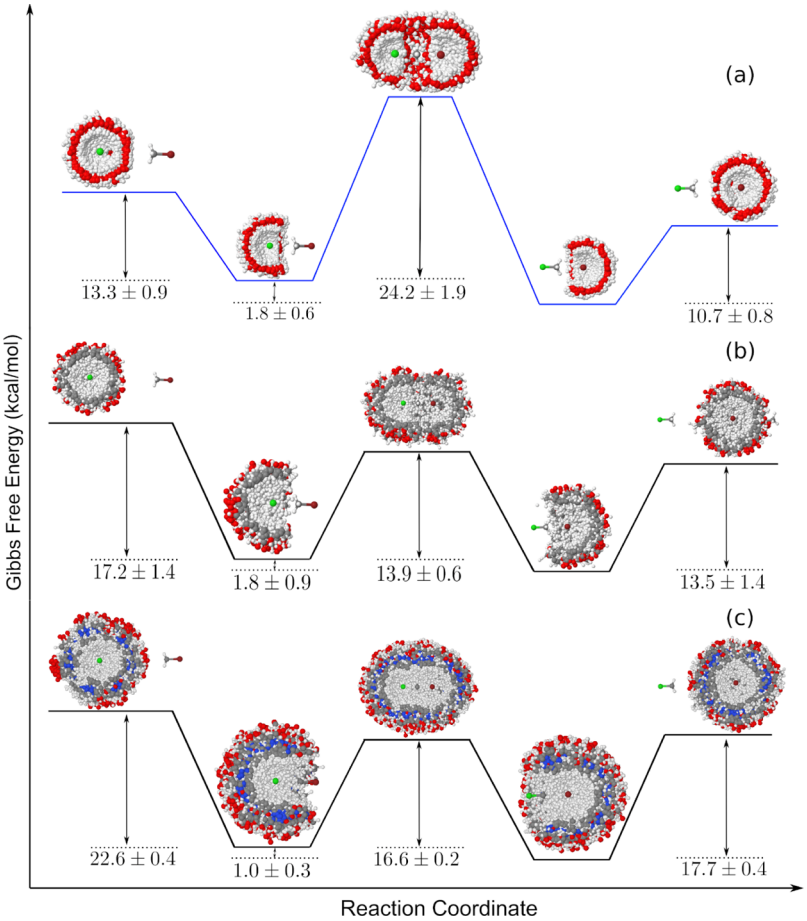

Figure 3. Gibbs free-energy difference for the reaction complex in (a) water, (b) acetone, and (c) dimethylformamide. The accessible volume of the closest solvent molecules at each relevant point of the reaction is also illustrated.

https://doi.org/10.1021/acs.jpcb.1c10282
J. Phys. Chem. B 2022, 126, 3685−3692

Table 5. Enthalpy, Gibbs Free Energy, and Entropy Difference along Some Phases of the $CH_3Br + Cl^- \rightarrow CH_3Cl + Br^-$ Reaction in Dimethylformamide, Acetone, and Water

solvent		reactant → shell (Cl)	reactant → TS	TS → product	product → shell (Br)
DMF	ΔH	−36.6 ± 0.7	7.4 ± 0.5	−2.5 ± 0.8	−12.8 ± 0.7
	ΔG	22.6 ± 0.4	16.6 ± 0.2	−17.6 ± 0.2	17.7 ± 0.4
	$T\Delta S$	−59.2 ± 1.1	−9.2 ± 0.7	15.1 ± 1.0	−30.5 ± 1.1
ACE	ΔH	−5.7 ± 0.3	79.4 ± 0.3	−1.3 ± 0.3	−0.7 ± 0.3
	ΔG	17.2 ± 1.4	13.9 ± 0.6	−15.2 ± 0.3	13.5 ± 1.4
	$T\Delta S$	−22.9 ± 1.7	65.5 ± 0.9	13.9 ± 0.6	−14.2 ± 1.7
WAT	ΔH	−11.1 ± 0.9	23.3 ± 0.4	−10.6 ± 0.4	−4.6 ± 0.6
	ΔG	13.3 ± 0.9	24.2 ± 1.9	−26.0 ± 0.3	10.7 ± 0.8
	$T\Delta S$	2.2 ± 1.8	−0.9 ± 2.5	9.4 ± 0.7	−15.3 ± 1.4

dimethylformamide, which implies that both the reactant and product are more stabilized in these environments. Thus, in all solvents, the chlorine and bromine ions prefer to make HBs interact with bromomethane or chloromethane than with the solvent molecules; that is, the process is spontaneous. Another remark is that a full solvation shell is observed around the TS, but it is less structured in ACE (Figure 3).

3.4. Entropy Profile. Another issue concerns the entropy contribution along with the relevant points of the reaction. This can be derived from our simulations using the thermodynamic equation that relates the variations of free energy (ΔG), enthalpy (ΔH), and entropy (ΔS). It is worth mentioning that the vibrational contribution is not included in our model because the molecules are kept rigid during the classical simulations. Nonetheless, other contributions (electronic, rotational, and translational) are taken into account. Notably, the vibrational, rotational, and translational contributions can be estimated using low-cost approaches based on continuum models, for instance, the COSMO-RS[71,72] (conductor-like screening model for real solvents) approach, but these contributions to the Gibbs free-energy barriers are not expected to be significant in this study. This is emphasized by noting the large calculated energy barriers that will not change appreciably by the small differences in entropy of the specific points. The configurational enthalpy difference (ΔH_c) depends on the solute−solvent and solvent−solvent interactions, with the latter term usually being called in the literature as solvent relaxation energy. This quantity has a slow convergence because it is computed from the fluctuation between two large numbers,[73] which demands extremely large MC simulations to achieve convergence. The convergence procedure for all solvents is illustrated in Figure S1 in the Supporting Information, and Table 4 shows the converged values of the variations of free energy, enthalpy, and entropy involving many stages of the $CH_3Br + Cl^- \rightarrow CH_3Cl + Br^-$ reaction.

As we can see in Table 5, the ΔH and $T\Delta S$ values for the reactant → shell (Cl) and product → shell (Br) are always negative (except $T\Delta S$ in water), with DMF having the most extreme values. As entropy is directly related to the disorder degree, we can deduce that the full solvation shell around the ions leads to a more organized structure than the minima (reactant and product). Except for ACE, the entropy decreases from the reactant to TS and increases from TS to the product. Overall, the entropy contribution in water is relatively small.

4. CONCLUSIONS

This work has been devoted to the study of the liquid solvent effects on S_N2 reaction. Theoretical advances were made by obtaining the Gibbs free energy along the reaction path and at specific important points, such as the transition state. Explicit solvent molecules were included that obeyed thermodynamic conditions and the distribution derived from a Monte Carlo simulation. A systematic study of the $CH_3Br + Cl^- \rightarrow CH_3Cl + Br^-$ reaction was carried out in gas and in three solvent environments. To this end, several ground-state critical points along the reaction path were optimized (minima and transition states). The estimation of the activation energy barrier by using FEP calculations indicates an increase in this property when the solvent is included, with theoretical predictions close to those measured experimentally. In addition, the reaction becomes less exothermic in solution because the reactant is energetically calculated to be around 1 kcal/mol above the product. This finding could be explained in water because the solute−solvent hydrogen bond interactions are more intense in the product than in the reactant. Finally, the entropic contributions are considerably small, mainly in aqueous solution. In all cases, we obtained a picture that agreed with the experiment for the three considered solvents. Hence, this study opens the possibility of realistic theoretical studies of chemical reactions in solution..

■ ASSOCIATED CONTENT

Supporting Information

The Supporting Information is available free of charge at https://pubs.acs.org/doi/10.1021/acs.jpcb.1c10282.

Configuration enthalpy difference evolution in (a) water, (b) acetone, and (c) dimethyformamide; energy difference between the transition state and reactant and the product and reactant calculated from several quantum chemistry methods; energy difference between the transition state and reactant and the product and reactant computed by changing the aug-cc-pVXZ (X = D, T, Q, and 5) basis set; selected parameters of the $CH_3Br + Cl^- \rightarrow CH_3Cl + Br^-$ reaction in its reactant, TS, and product structure; and Cartesian coordinates of the optimized structures (PDF)

■ AUTHOR INFORMATION

Corresponding Author

Danillo Valverde − *Instituto de Física, Universidade de São Paulo, 05508-090 São Paulo, São Paulo, Brazil;* Present Address: Now at Unité de Chimie Physique Théorique et Structurale & Laboratoire de Physique du Solid, Namur Institute of Structured Matter, Université de Namur, B-5000 Namur, Belgium; orcid.org/0000-0002-1893-4579; Email: danillo.piresvalverde@unamur.be

https://doi.org/10.1021/acs.jpcb.1c10282
J. Phys. Chem. B 2022, 126, 3685−3692

Authors

Herbert C. Georg − *Instituto de Física, Universidade Federal de Goiás, 74690-900 Goiânia, Goiás, Brazil*

Sylvio Canuto − *Instituto de Física, Universidade de São Paulo, 05508-090 São Paulo, São Paulo, Brazil;* orcid.org/0000-0002-9942-8714

Complete contact information is available at: https://pubs.acs.org/10.1021/acs.jpcb.1c10282

Notes

The authors declare no competing financial interest.

■ ACKNOWLEDGMENTS

This work was supported by grants 2016/22723-2 and 2017/02612-4 from the São Paulo Research Foundation (FAPESP). The authors thank the Brazilian funds CNPq, CAPES, and the computational resources provided by HPC through Superintendência de Tecnologia da Informação da Universidade de São Paulo. S.C. also acknowledges CAPES for the Biomol project 23038.004630/2014-35 and the National Institute of Science and Technology Complex Fluids (INCT-FCx) with the CNPq grant 141260/2017-3 and FAPESP grant 2014/50983-3.

■ REFERENCES

(1) Hase, W. L. Simulations of Gas-Phase Chemical Reactions: Applications to S N 2 Nucleophilic Substitution. *Science* **1994**, *266*, 998−1002.

(2) Chabinyc, M. L.; Craig, S. L.; Regan, C. K.; Brauman, J. I. Gas-phase ionic reactions: Dynamics and mechanism of nucleophilic displacements. *Science* **1998**, *279*, 1882−1886.

(3) Xie, J.; Hase, W. L. Rethinking the SN2 reaction. *Science* **2016**, *352*, 32−33.

(4) Hennig, C.; Schmatz, S. Four-dimensional quantum study on exothermic complex-forming reactions: Cl−+CH3Br→ClCH3+Br−. *J. Chem. Phys.* **2005**, *122*, 234307.

(5) Schmatz, S.; Botschwina, P.; Stoll, H. Coupled cluster calculations for the SN2 reaction Cl− + CH3Br → ClCH3 + Br−. *Int. J. Mass Spectrom.* **2000**, *201*, 277−282.

(6) Raugei, S.; Cardini, G.; Schettino, V. An ab initio molecular dynamics study of the SN2 reaction Cl−+CH3Br→CH3Cl+Br−. *J. Chem. Phys.* **1999**, *111*, 10887−10894.

(7) Manikandan, P.; Zhang, J.; Hase, W. L. Chemical Dynamics Simulations of X- + CH3Y → XCH3 + Y- Gas-Phase SN2 Nucleophilic Substitution Reactions. Nonstatistical Dynamics and Nontraditional Reaction Mechanisms. *J. Phys. Chem. A* **2012**, *116*, 3061−3080.

(8) Pratihar, S.; Ma, X.; Homayoon, Z.; Barnes, G. L.; Hase, W. L. Direct chemical dynamics simulations. *J. Am. Chem. Soc.* **2017**, *139*, 3570−3590.

(9) Angel, L. A.; Garcia, S. P.; Ervin, K. M. Dynamics of the gas-phase reactions of chloride ion with fluoromethane: High excess translational activation energy for an endothermic SN2 reaction. *J. Am. Chem. Soc.* **2002**, *124*, 336−345.

(10) Szabó, I.; Császár, A. G.; Czakó, G. Dynamics of the F− + CH3Cl → Cl− + CH3F SN2 reaction on a chemically accurate potential energy surface. *Chem. Sci.* **2013**, *4*, 4362−4370.

(11) Mikosch, J.; Trippel, S.; Eichhorn, C.; Otto, R.; Lourderaj, U.; Zhang, J. X.; Hase, W. L.; Weidemüller, M.; Wester, R. Imaging nucleophilic substitution dynamics. *Science* **2008**, *319*, 183−186.

(12) Szabó, I.; Czakó, G. Revealing a double-inversion mechanism for the F^-+CH3Cl SN2 reaction. *Nat. Commun.* **2015**, *6*, 5972.

(13) Olasz, B.; Czakó, G. High-Level-Optimized Stationary Points for the F-(H2O) + CH3I System: Proposing a New Water-Induced Double-Inversion Pathway. *J. Phys. Chem. A* **2018**, *123*, 454−462.

(14) Laerdahl, J. K.; Uggerud, E. Gas phase nucleophilic substitution. *Int. J. Mass Spectrom.* **2002**, *214*, 277−314.

(15) Bogdanov, B.; McMahon, T. B. Thermochemistry and structures of solvated SN2 complexes and transition states in the gas phase: experiment and theory. *Int. J. Mass Spectrom.* **2005**, *241*, 205−223.

(16) Vöhringer-Martinez, E.; Hansmann, B.; Hernandez, H.; Francisco, J.; Troe, J.; Abel, B. Water catalysis of a radical-molecule gas-phase reaction. *Science* **2007**, *315*, 497−501.

(17) Chandrasekhar, J.; Smith, S. F.; Jorgensen, W. L. SN2 reaction profiles in the gas phase and aqueous solution. *J. Am. Chem. Soc.* **1984**, *106*, 3049−3050.

(18) Bohme, D. K.; Mackay, G. I. Bridging the gap between the gas phase and solution: Transition in the kinetics of nucleophilic displacement reactions. *J. Am. Chem. Soc.* **1981**, *103*, 978−979.

(19) Vayner, G.; Houk, K. N.; Jorgensen, W. L.; Brauman, J. I. Steric retardation of SN2 reactions in the gas phase and solution. *J. Am. Chem. Soc.* **2004**, *126*, 9054−9058.

(20) Xu, Y.; Zhang, J.; Wang, D. Investigation of the CH3Cl + CN− reaction in water: Multilevel quantum mechanics/molecular mechanics study. *J. Chem. Phys.* **2015**, *142*, 244505.

(21) Satpathy, L.; Sahu, P. K.; Behera, P. K.; Mishra, B. K. Solvent Effect on the Potential Energy Surfaces of the F- + CH3CH2Br Reaction. *J. Phys. Chem. A* **2018**, *122*, 5861−5869.

(22) Zhang, J.; Yang, L.; Xie, J.; Hase, W. L. Microsolvated F-(H2O) + CH3I SN2 Reaction Dynamics. Insight into the Suppressed Formation of Solvated Products. *J. Phys. Chem. Lett.* **2016**, *7*, 660−665.

(23) Liu, X.; Xie, J.; Zhang, J.; Yang, L.; Hase, W. L. Steric effects of solvent molecules on SN2 substitution dynamics. *J. Phys. Chem. Lett.* **2017**, *8*, 1885−1892.

(24) Liu, X.; Yang, L.; Zhang, J.; Sun, J. Competition of F/OH-Induced SN2 and Proton-Transfer Reactions with Increased Solvation. *J. Phys. Chem. A* **2018**, *122*, 9446−9453.

(25) Gu, M.; Liu, X.; Yang, L.; Sun, S.; Zhang, J. Dynamics of Cl-(H2O) + CH3I Substitution Reaction: The Influences of Solvent and Nucleophile. *J. Phys. Chem. A* **2019**, *123*, 2203−2210.

(26) Miertuš, S.; Scrocco, E.; Tomasi, J. Electrostatic interaction of a solute with a continuum. A direct utilization of AB initio molecular potentials for the prevision of solvent effects. *Chem. Phys.* **1981**, *55*, 117−129.

(27) Klamt, A.; Schüürmann, G. COSMO: A new approach to dielectric screening in solvents with explicit expressions for the screening energy and its gradient. *J. Chem. Soc., Perkin Trans. 2* **1993**, 799−805.

(28) Tu, Y.; Laaksonen, A. Implementing Quantum Mechanics into Molecular Mechanics-Combined QM/MM Modeling Methods. *Advances in Quantum Chemistry*; Sabin, J. R., Brandas, E., Canuto, S., Eds.; Elsevier: Netherlands, 2010; Vol. *59*, pp 1−15.

(29) Coutinho, K.; Rivelino, R.; Georg, H. C.; Canuto, S. The Sequential qm/mm Method and its Applications to Solvent Effects in Electronic and Structural Properties of Solutes. In *Solvation Effects on Molecules and Biomolecules: Computational Methods and Applications*; Canuto, S., Ed.; Springer Netherlands: Dordrecht, 2008; pp 159−189.

(30) Okuyama-Yoshida, N.; Nagaoka, M.; Yamabe, T. Transition-state optimization on free energy surface: Toward solution chemical reaction ergodography. *Int. J. Quantum Chem.* **1998**, *70*, 95−103.

(31) Nagaoka, M. Structure optimization of solute molecules via Free Energy Gradient method. *Bull. Kor. Chem. Soc.* **2003**, *24*, 805−808.

(32) Coutinho, K.; Georg, H. C.; Fonseca, T. L.; Ludwig, V.; Canuto, S. An efficient statistically converged average configuration for solvent effects. *Chem. Phys. Lett.* **2007**, *437*, 148−152.

(33) Georg, H. C.; Canuto, S. Electronic properties of water in liquid environment. A sequential QM/MM study using the free energy gradient method. *J. Phys. Chem. B* **2012**, *116*, 11247−11254.

(34) Franco, L. R.; Brandão, I.; Fonseca, T. L.; Georg, H. C. Elucidating the structure of merocyanine dyes with the ASEC-FEG method. Phenol blue in solution. *J. Chem. Phys.* **2016**, *145*, 194301.

(35) Bistafa, C.; Georg, H. C.; Canuto, S. Combining ab initio multiconfigurational and Free Energy Gradient methods to study the π-π^* excited state structure and properties of uracil in water. *Comput. Theor. Chem.* **2014**, *1040−1041*, 312−320.

(36) Ludwig, V.; da Costa Ludwig, Z. M.; Valverde, D.; Georg, H. C.; Canuto, S. Free energy gradient for understanding the stability and properties of neutral and charged L-alanine molecule in water. *J. Mol. Liq.* **2020**, *319*, 114109.
(37) Brandão, I.; Fonseca, T. L.; Georg, H. C.; Castro, M. A.; Pontes, R. B. Assessing the structure and first hyperpolarizability of Li@B10H14 in solution: a sequential QM/MM study using the ASEC-FEG method. *Phys. Chem. Chem. Phys.* **2020**, *22*, 17314−17324.
(38) Sanches de Araújo, A. V.; Valverde, D.; Canuto, S.; Borin, A. C. Solvation Structures and Deactivation Pathways of Luminescent Isothiazole-Derived Nucleobases: tzA, tzG, and tzI. *J. Phys. Chem. A* **2020**, *124*, 6834−6844.
(39) Cezar, H. M.; Canuto, S.; Coutinho, K. Solvent effect on the syn/anti conformational stability: A comparison between conformational bias Monte Carlo and molecular dynamics methods. *Int. J. Quantum Chem.* **2019**, *119*, No. e25688.
(40) Glukhovtsev, M. N.; Bach, R. D.; Pross, A.; Radom, L. The performance of B3-LYP density functional theory in describing SN2 reactions at saturated carbon. *Chem. Phys. Lett.* **1996**, *260*, 558−564.
(41) Seeley, J. V.; Morris, R. A.; Viggiano, A. A.; Wang, H.; Hase, W. L. Temperature Dependence of the Rate Constants and Branching Ratios for the Reactions of Cl-(D2O)1-3 with CH3Br and Thermal Dissociation Rates for Cl-(CH3Br). *J. Am. Chem. Soc.* **1997**, *119*, 577−584.
(42) Bathgate, R. H.; Moelwyn-Hughes, E. A. 530. The kinetics of certain ionic exchange reactions of the four methyl halides in aqueous solution. *J. Chem. Soc.* **1959**, 2642−2648.
(43) Zhang, H.; Liu, B.; Wang, L.; Li, Z.-s.; Liu, J.-y.; Yu, X.-y.; Sun, C.-c. Ab initio direct dynamic study on the reaction Br atoms with CH3Br. *Chem. Phys. Lett.* **2006**, *420*, 12−17.
(44) Schmatz, S. Quantum dynamics of SN2 reactions on CCSD(T) potential energy surfaces: Cl−+CH3Cl and Cl−+CH3Br. *Chem. Phys. Lett.* **2000**, *330*, 188−194.
(45) Raugei, S.; Cardini, G.; Schettino, V. Microsolvation effect on chemical reactivity: The case of the Cl−+CH3Br SN2 reaction. *J. Chem. Phys.* **2001**, *114*, 4089−4098.
(46) Pagliai, M.; Raugei, S.; Cardini, G.; Schettino, V. Car-Parrinello molecular dynamics on the SN2 reaction Cl−+CH3Br in water. *J. Mol. Struct.* **2003**, *630*, 141−149.
(47) Alexander, R.; Ko, E. C. F.; Parker, A. J.; Broxton, T. J. Solvation of ions. XIV. Protic-dipolar aprotic solvent effects on rates of bimolecular reactions. Solvent activity coefficients of reactants and transition states at 25°. *J. Am. Chem. Soc.* **1968**, *90*, 5049−5069.
(48) Cook, D.; Parker, A. J. Halide exchange at a saturated carbon atom in dimethylformamide solvent. Comparison of experimental rates and Arrhenius parameters with values calculated by Ingold. *J. Chem. Soc.* **1968**, 142−148.
(49) Parker, A. J. Protic-dipolar aprotic solvent effects on rates of bimolecular reactions. *Chem. Rev.* **1969**, *69*, 1−32.
(50) Møller, C.; Plesset, M. S. Note on an approximation treatment for many-electron systems. *Phys. Rev.* **1934**, *46*, 618−622.
(51) Kendall, R. A.; Dunning, T. H., Jr; Harrison, R. J. Electron affinities of the first-row atoms revisited. Systematic basis sets and wave functions. *J. Chem. Phys.* **1992**, *96*, 6796−6806.
(52) Galván, I. F.; Muñoz-Losa, A.; Soriano-Correa, C.; Luz Sánchez, M.; Elena Martín, M.; Aguilar, M. A. Use of the average solvent potential approach in the study of solvent effects. *Advances in Quantum Chemistry*; Sabin, J. R., Brandas, E., Canuto, S., Eds.; Elsevier: Netherlands, 2010; Vol. *59*, pp 59−97.
(53) Georg, H. C.; Fernandes, T. S.; Canuto, S.; Takenaka, N.; Kitamura, Y.; Nagaoka, M. A combination of the sequential QM/MM and the free energy gradient methodologies with applications. In *Practical Aspects of Computational Xhemistry III*; Leszczynski, J., Shukla, M. K., Eds.; Springer: New York, 2014; pp 231−247.
(54) Metropolis, N.; Rosenbluth, A. W.; Rosenbluth, M. N.; Teller, A. H.; Teller, E. Equation of state calculations by fast computing machines. *J. Chem. Phys.* **1953**, *21*, 1087−1092.
(55) Jorgensen, W. L.; Maxwell, D. S.; Tirado-Rives, J. Development and testing of the OPLS all-atom force field on conformational energetics and properties of organic liquids. *J. Am. Chem. Soc.* **1996**, *118*, 11225−11236.
(56) Singh, U. C.; Kollman, P. A. An approach to computing electrostatic charges for molecules. *J. Comput. Chem.* **1984**, *5*, 129−145.
(57) Jorgensen, W. L.; Briggs, J. M.; Contreras, M. L. Relative partition coefficients for organic solutes from fluid simulations. *J. Phys. Chem.* **1990**, *94*, 1683−1686.
(58) Chalaris, M.; Samios, J. A molecular dynamics simulation study of Li+-Cl− ion pair dissolved in DMF (-d7). *J. Mol. Liq.* **1998**, *78*, 201−215.
(59) Berendsen, H. J. C.; Grigera, J. R.; Straatsma, T. P. The missing term in effective pair potentials. *J. Phys. Chem.* **1987**, *91*, 6269−6271.
(60) Canuto, S.; Coutinho, K. From hydrogen bond to bulk: Solvation analysis of then-?* transition of formaldehyde in water. *Int. J. Quantum Chem.* **2000**, *77*, 192−198.
(61) Zwanzig, R. W. High-Temperature Equation of State by a Perturbation Method. I. Nonpolar Gases. *J. Chem. Phys.* **1954**, *22*, 1420−1426.
(62) Cezar, H. M.; Canuto, S.; Coutinho, K. DICE: A Monte Carlo Code for Molecular Simulation Including the Configurational Bias Monte Carlo Method. *J. Chem. Inf. Model.* **2020**, *60*, 3472−3488.
(63) Frisch, M. J.; Trucks, G. W.; Schlegel, H. B.; Scuseria, G. E.; Robb, M. A.; Cheeseman, J. R.; Scalmani, G.; Barone, V.; Petersson, G. A.; Nakatsuji, H.; et al. *Gaussian 09* Revision E.01.; Gaussian Inc.: Wallingford CT, 2009.
(64) Yu, F. Dynamic exit-channel pathways of the microsolvated HOO−(H2O) + CH3Cl SN2 reaction: Reaction mechanisms at the atomic level from direct chemical dynamics simulations. *J. Chem. Phys.* **2018**, *148*, 014302.
(65) Li, C.; Liu, P.; Li, Y.; Wang, D. Solvent effects and potential of mean force study of the S N 2 reaction of CH 3 +CN − in water. *Chin. Phys. B* **2018**, *27*, 033401.
(66) Mezei, M.; Beveridge, D. L. Theoretical studies of hydrogen bonding in liquid water and dilute aqueous solutions. *J. Chem. Phys.* **1981**, *74*, 622−632.
(67) Swiatla-Wojcik, D. Evaluation of the criteria of hydrogen bonding in highly associated liquids. *Chem. Phys.* **2007**, *342*, 260−266.
(68) Coutinho, K.; Canuto, S. The sequential Monte Carlo-quantum mechanics methodology. Application to the solvent effects in the Stokes shift of acetone in water. *THEOCHEM* **2003**, *632*, 235−246.
(69) Satpathy, L.; Sahoo, S.; Sahu, P. K.; Behera, P. K.; Mishra, B. K. Effect of solvent polarity on the potential energy surface in the SN2 reaction of F− + CH3Cl. *Comput. Theor. Chem.* **2019**, *1150*, 18−25.
(70) Higashi, M.; Truhlar, D. G. Combined electrostatically embedded multiconfiguration molecular mechanics and molecular mechanical method: Application to molecular dynamics simulation of a chemical reaction in aqueous solution with hybrid density functional theory. *J. Chem. Theory Comput.* **2008**, *4*, 1032−1039.
(71) Klamt, A.; Eckert, F. COSMO-RS: a novel and efficient method for the a priori prediction of thermophysical data of liquids. *Fluid Phase Equilib.* **2000**, *172*, 43−72.
(72) Klamt, A.; Eckert, F. Prediction of vapor liquid equilibria using COSMOtherm. *Phase Equil.* **2004**, *217*, 53−57.
(73) Lazaridis, T. Solvent reorganization energy and entropy in hydrophobic hydration. *J. Phys. Chem. B* **2000**, *104*, 4964−4979.

https://doi.org/10.1021/acs.jpcb.1c10282
J. Phys. Chem. B 2022, 126, 3685−3692